Accepted Manuscript

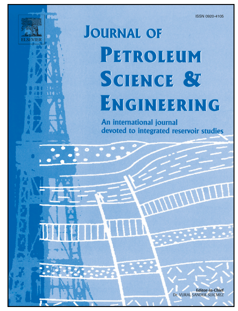

Experimental investigation on the impact of coal fines generation and migration on coal permeability

Tianhang Bai, Zhongwei Chen, Saiied M. Aminossadati, Thomas E. Rufford, Ling Li

PII: S0920-4105(17)30734-9

DOI: 10.1016/j.petrol.2017.09.035

Reference: PETROL 4278

To appear in: *Journal of Petroleum Science and Engineering*

Received Date: 20 June 2017

Revised Date: 13 September 2017

Accepted Date: 17 September 2017

Please cite this article as: Bai, T., Chen, Z., Aminossadati, S.M., Rufford, T.E., Li, L., Experimental investigation on the impact of coal fines generation and migration on coal permeability, *Journal of Petroleum Science and Engineering* (2017), doi: 10.1016/j.petrol.2017.09.035.

Experimental Investigation on the Impact of Coal Fines Generation and Migration on Coal Permeability

Tianhang Bai[1], Zhongwei Chen[1,*], Saiied M. Aminossadati[1], Thomas E. Rufford[2], Ling Li[3]

[1]*School of Mechanical and Mining Engineering, the University of Queensland, QLD 4072, Australia*
[2]*School of Chemical Engineering, the University of Queensland, QLD 4072, Australia*
[3]*School of Civil Engineering, the University of Queensland, QLD 4072, Australia*
**Corresponding author email address: zhongwei.chen@uq.edu.au*

ABSTRACT

Measurements of the coal fines production and the impact of these fines on the permeability of two coals from the Bowen Basin, Australia, were performed at different flow conditions (single-phase water or gas, two-phase water and gas) and pressure conditions. The fines collected from each coal samples ranged in size from 1 μm to 14 μm. For both coal samples, during the first 50 hours, the permeability decreases from 0.005 mD and 0.048 mD by 60.9% and 85%, respectively, followed by gradual decline with fluctuations. By the end of water injection, the permeability drops by 88% and 89%, respectively. This phenomenon is attributed to the counteraction between formation damage (cleats plugging and coal fines settlement) and breakthrough of coal fines from the samples (widened cleats). It was found that coal fines volumetric production is proportional to the third power of flow velocity once the flow paths for coal fines are established. The critical flow velocities of coal fines production for both samples were also obtained. For hydrophobic coal, water-drive-gas two-phase flow introduces abrupt permeability loss due to coal fines generation and migration. Furthermore, pauses (well shut-in) in the experiments cause slight permeability drops. A comparison between the two samples indicates that narrower and less connected cleating system results in more frequent coal fines generation and migration, resulting in significant permeability fluctuations with general decreasing trend. Tortuosity of the cleats can enhance the deterioration in permeability by coal fines behaviours. This study delivers fundamental understandings of coal fines generation and migration during the CSG production process, and useful guidelines are suggested to be implemented in the field to minimize production loss induced by coal fines behaviours.

Keywords: Coal fines generation and migration; Core flooding; Permeability variation; Critical velocity; Cleat structure

1 INTRODUCTION

Coal fines are produced from coal seam gas (CSG) reservoirs throughout the CSG production process. The size of coal fines collected in CSG wells varies from a few nanometres diameter to hundreds of microns. These fines have detrimental impacts on CSG production, such as formation damage and pump failures (Marcinew and Hinkel, 1990; Nimerick et al., 1990). A small portion of coal fines naturally exists in virgin coal cleats; while a large portion is generated mainly by fluid flushing and pressure disturbance (Yao et al., 2016). During the CSG production process, when different flow regimes take place (e.g. single-phase flow and two-phase flow) (Bai et al., 2017; Wang et al., 2017), coal fines may plug coal cleats and/or deposit in cleats during the migration process, deteriorating coal permeability. This results in significant drop in the gas productivity (Magill et al., 2010; Palmer et al., 2005). In addition, coal fines can migrate towards a CSG well, burying the downhole pumps, after which workovers will be required to resume the production process (Black, 2011; Okotie and Moore, 2010). Appropriate production strategies can alleviate the coal fines induced problems according to different reservoir conditions.

Mathematical models using force and stress balance analysis have been used in several studies (Bedrikovetsky et al., 2011; Khilar and Fogler, 1998; Moore et al., 2011) to predict coal fines generation and attempt to identify the factors that influence fines generation. The two forces considered as the main causes for coal fines breakage and migration in coal cleats are the hydrodynamic forces and the colloidal forces. Coal fines start to detach from coal cleats as the hydrodynamic force exceeds the colloidal force (Bedrikovetsky et al., 2011; Khilar and Fogler, 1998). The particle rotation effect is taken into account in the force balance model (Bedrikovetsky et al., 2011). However, the rotation effect can be neglected given the small sizes of coal fines (less than 100 μm). Instead, the stress analysis suggests that both shear failure (Palmer et al., 2005) and tensile failure (Moore et al., 2011) are possible failure mechanisms when the stress balance is breached.

In our previous paper (Bai et al., 2015), we numerically simulated coal fines generation during the dewatering phase. The results reveal that coal fines start to be generated as the pressure gradient reaches a critical value, which is dependent on cleat geometries. More coal fines are generated as the pressure gradient increased. We also conducted two-phase flow simulations (Bai et al., 2016; Bai et al., 2017). We find that two-phase flow generates more coal fines compared to single-phase flow. It is suggested that in order to reduce coal fines production, frequently well shut-in should be avoided. Although the generation of coal fines has been linked to different cleat geometries, the permeability evolution associated with coal fines generation remains poorly understood.

Gash (1991) experimentally tested core flooding behaviours to evaluate the impact of coal fines on permeability, and confirmed the formation damage was due to coal fines migration, because he observed the permeability recovery when the flow direction was reversed. Yao et al. (2016) used reconstituted coal samples to investigate the effect of tectonically deformed coal types on the characteristics of coal fines generation. They suggest that granulated coal is more sensitive to flow velocity and reservoir effective stress than the undeformed coal, but the permeability variations were not measured in their experiments. Wei et al. (2015) experimentally demonstrated the critical flux for coal fines generation, and proposed a maximum water production for a particular CSG well. Guo et al. (2015, 2016) conducted a series of core flooding tests using water to quantify the permeability variations caused by coal fines production. They conclude that the variation of permeability generally matches with the trend of coal fines production (i.e. more significant permeability drop corresponding to more coal fines production), and the permeability decreases continuously.

From the field trials from 12 CSG wells, Zhao et al. (2016) observed that coal fines emerged during the water production stage ranged from 10 μm to 100 μm, and higher water flow rate led to more severe damage to CSG reservoirs. Wei et al. (2013) further investigated the characteristics of coal fines production in a gas field in China. From the samples collected from the CSG wells at different production stages, they found that the size of coal fines was greater during the dewatering of coal seams, and the coal fines production was higher for both dewatering and initial production (two-phase flow) phases. In these field trials, the permeability of the coal seams has not been quantified to correspond to the coal fines behaviours.

The impact of production parameters (e.g. water flow velocity and production pressure) on coal fines generation and permeability has been reported by researchers. However, the relationship between the characteristics of coal fines behaviours and permeability variations for different CSG production scenarios has not been comprehensively investigated. This relationship offers a vital knowledge for addressing the coal fines issues. Besides, the effects of gravity and cleat structure on such relationship have not been accounted for in previous research (Zhao et al., 2017).

In this study, laboratory experiments will be performed using two samples to examine coal permeability changes due to coal fines generation and migration at various production scenarios, including single-phase flow, two-phase flow and well shut-in. The correlation between the characteristics of coal fines and permeability variations will be established and the implications for managing coal fines challenges in the field will be discussed in detail. The effects of gravity and cleat structure on the fines-permeability relationship will also be investigated.

2 EXPERIMENTAL METHODOLOGY

2.1 Sample preparation

Two 3 cm cubes were cut from a piece of coal collected from a coal mine in the Bowen Basin (Australia), as shown in Fig. 1a. The contact angles measured with water on the two coal samples using a Sessile Drop experiment were 116° and 109°, which suggests these coals tend to segregate from water (i.e. hydrophobic). Each coal sample was cast in a cylinder of resin to simulate constrained reservoir boundary conditions (Fig. 1b). Resin fluid distributors with the same cross-sectional size as the cubic sample were made and placed at each end of the samples and a 1/4" tube was embedded directly in each distributor to serve as the fluid conduit. Any small gaps between the cubic sample and the fluid distributors were sealed laterally to prevent leakage. The coal cubes were orientated with the bedding planes parallel to the fluid conduits so that the flow direction was most closely aligned to the face cleats.

Fig. 1. (a) The coal sample and (b) the resin coated sample.

2.2 Sample characterization

The sample characterization includes Scanning Electron Microscopy (SEM) to visualize the cleating system; X-ray Diffraction (XRD) to examine the mineral contents; Mercury Intrusion Porosimetry (MIP) to quantify the initial porosity; and flooding test to obtain the initial permeability. The former three types of characterization were obtained using the debris from the two coal samples. Since the debris came off from different spots of the samples, we would say the characterization obtained was representative of the whole samples.

The JEOL 7800 SEM was used to take images focusing on the cleat aperture and connectivity for both coal samples. We looked at three fragments from each coal sample, and all of them exhibited similar characteristics for each sample. Therefore, we chose one from them to illustrate the representative characteristics, as shown in Fig. 2 and Fig. 3. Fig. 2a and Fig. 3a show a typical face cleat in Sample 1 and Sample 2, respectively. Both face cleats are continuous, but the one in Sample 2 is more tortuous. Fig. 2b and Fig. 3b better demonstrate the connectivity of coal cleats, and the butt cleats in Sample 2 are better developed and connected with each other. When it comes down to a higher resolution, it can be seen that the aperture of the face cleat is wider in Sample 2 (14 μm) compared with that in Sample 1 (7 μm). The characteristics of the coal cleats in both samples are summarised in Table 1.

Fig. 2. SEM images for Sample 1.

Fig. 3. SEM images for Sample 2.

Table 1. Qualitative comparison of coal cleats for both coal samples from the Bowen Basin.

	Sample 1	**Sample 2**

Tortuosity	Flat	Tortuous
Connectivity	Poor	Good
Aperture	Narrow	Wide

The X-ray Powder Diffraction (XRD) tests were performed using the Bruker D8 Advance Powder X-ray diffractometer, and the results are demonstrated in Fig. 4. It can be seen that the two coal samples possess similar mineral contents, which mainly includes kaolinite, with some quartz. Few swelling minerals are present in the coal samples, hence the swelling effect on coal permeability can be neglected.

Fig. 4. XRD test results of both coal samples.

The initial porosity of the samples was evaluated by Mercury Intrusion Porosimetry (MIP) using the Micromeritics AutoPore IV9520, and the initial permeability was obtained at the beginning of the flow tests. The tested values are listed in Table 2. The MIP curves are plotted in Fig. 5. In order to correspond to the size of coal fines, which will be displayed afterwards, the pore size distribution analysis was focused on the zone of interest (0.6 μm to 14 μm). There are more pores and fractures in Sample 2 for the majority of the size range, and this is the case in the zone of interest, which confirms the observations in the SEM images. The initial porosity and permeability of the samples coincide with the characterization of the cleats (Table 1). To be more specific, better connected and wider cleats give rise to higher initial porosity and permeability.

Table 2. Initial porosity and permeability of both coal samples.

	Sample 1	**Sample 2**
Initial porosity (%)	4.73	9.08
Initial permeability (mD)	0.005	0.048

Fig. 5. MIP curves for both samples (a) pore size distribution from 0.01 μm to 100 μm; and (b) pore size distribution in the zone of interest (0.6 μm to 14 μm).

2.3 Core flooding rig

The ISCO 500D syringe pump was used to inject water and helium vertically through the assembled samples at constant differential pressures (i.e. $\Delta P = P_1 - P_2$ is constant, where P_1 is the inlet pressure and P_2 is the outlet pressure). The outlet was open to the atmosphere. No external confining stress was applied to the samples. The fluid flow rate and pump pressure were logged, and used to calculate the change in permeability.

The permeability of water and gas were calculated using Eq (1) and Eq (2), respectively, based on Darcy's Law (Fu et al., 2009; Wei et al., 2015):

$$k_w = \frac{Q\mu_w L}{A(P_1 - P_2)} \tag{1}$$

$$k_g = \frac{2P_0 Q\mu_g L}{A(P_1^2 - P_2^2)} \tag{2}$$

where k_w and k_g are the permeabilities for water and gas, respectively. Q is the flow rate. μ_w and μ_g are the viscosities of water and gas, respectively. L is the length and A is the cross-sectional area of the sample. P_0 is atmospheric pressure.

2.4 Experiment scenarios

The experiment scenarios are illustrated in Fig. 6. For both coal samples, initially, water was used as the injection fluid to simulate the dewatering process. The pressure difference across the sample was set at 0.8 MPa, and it was increased by 0.1 MPa at each step until the pressure difference reached 1.5 MPa, and the change in pressure difference aims to examine its impact on coal fines production and corresponding permeability variations. Then helium gas was introduced to mimic gas-drive-water two-phase flow scenario in CSG reservoirs. In order to initiate the two-phase flow, the pressure difference was set as 1.1 MPa with an increment of 0.1 MPa at each time till 1.3 MPa.

In addition to the above scenarios, some more cases were conducted on Sample 2, including water-drive-gas two-phase flow, horizontal water flooding (to investigate the gravitational effect on coal fines behaviours) and backflow test (to prove coal fines behaviours are the cause for permeability change). Please be noted that for 1.3 MPa, 1.4 MPa and 1.5 MPa of water flooding, the experiment was paused for 15 h between two effluent samples were collected at one pressure, before proceeding to the next injection scenario in order to evaluate the impact of well shut-in on coal fines production.

Fig. 6. Injection scenarios for both coal samples. Note: solid and dash lines indicate the sample was vertically and horizontally placed, respectively.

During the measurements, the effluent from the sample was collected continuously, and the particle size distribution of fines in every 5 mL collected was analysed in the Multisizer^{TM} 4 Particle Analyser (Coulter Counter). Three particle size distribution analyses were measured on each sample to test at least 100,000 particles, and the mean particle size distribution was computed from the three runs, after subtraction of the background particle count measured in the injection water.

3 RESULTS AND DISCUSSION

In this section, three key aspects will be discussed, namely the volume of the produced coal fines, the distribution of the size of coal fines, and the permeability evolution induced by coal fines generation and migration.

3.1 Volume of coal fines

The total volume of coal fines production for every mL effluent for both coal samples was estimated and plotted in Fig. 7.

Fig. 7. Incremental coal fines production for each scenario of both samples. In the legend, “0.8 MPa” represents the pressure difference, “after gas” means water was re-injected after gas flooding, “flat” means that the sample was placed horizontally instead of vertically, and “backflow” indicates that the flow direction was reversed. The same convention applies for other figures of this work.

Sample 1 witnessed the peak yield of coal fines at 0.8 MPa, with the coal fines output at a comparable level for other subsequent scenarios. Since the coal fines production was high at the very first run (0.8 MPa), it can be deduced that such pressure different enables the sample to offer clear migration pathways for coal fines. Whereas coal fines did not gain flow paths for Sample 2 until the differential pressure reached 1.0 MPa, since the volume of coal fines in the effluent before 1.0 MPa was similar to that of the injection water. It can be inferred that there exists a threshold pressure, above which the passages for coal fines will be established. To be more specific, Sample 1 possesses a threshold pressure below 0.8 MPa; while the threshold for Sample 2 is around 1.0 MPa. The reason for a higher threshold for Sample 2 is the tortuosity of the cleats, greater tortuosity makes it more difficult for the fines to move, requiring a higher pressure for breakthrough. In addition, the outputs of coal fines from Sample 2 vary significantly during water flooding under various differential pressures, as illustrated in Fig. 7.

Bagnold (Bagnold, 1936) suggested that the mass transport of particles is proportional to the third power of the velocity, therefore, the relationship between the coal fines volumetric concentration and the third power of the absolute flow velocity during Stage 1 of the water injection was plotted in Fig. 8. The trend confirmed Bagnold’s finding, which means the coal fines production is proportional to the third power of the flow velocity (the results are not representative if clear flow paths for coal fines are not well established, thus, the 0.8 MPa and 0.9 MPa scenarios for Sample 2 were not accounted for when fitting the curve). The intersection of the fitted line and x-axis can be regarded as the third power of the critical velocity, which indicates that below the critical velocity, little coal fines would be produced (the red dot in Fig. 8). For these two samples, the predicted critical velocities were 0.82 μm/s and 5.49 μm/s, respectively. The following equations were employed to obtain the absolute flow velocity (Chen et al., 2010):

$$\frac{k}{k_0} = \left(\frac{\phi}{\phi_0}\right)^3 \quad (3)$$

$$v = \frac{Q}{A\phi} \quad (4)$$

where k and ϕ represent permeability and porosity of the coal sample, the subscription *0* indicates the initial status, and v is the absolute velocity.

Fig. 8. Proportional relationship between the coal fines volumetric concentration and flow velocity.

After Sample 2 being flooded by gas, water was then injected to displace gas to simulate the water-drive-gas two-phase flow scenario. Fig. 7 reveals that more coal fines are yielded under the two-phase flow conditions, as indicated by the red arrow. The possible reason is that a higher localised pressure gradient (resulted by local pressure build-up) (Bai et al., 2016) is required to overcome the capillary pressure to enable the breakthrough of two-phase flow, consequently more coal fines are created. When Sample 2 was laid down horizontally, less fines output was observed compared with that from the vertical position. Since the flow direction was parallel to the face cleats, and due to the gravitational effect, the coal sample when being placed horizontally is more prone to coal fines settlement issue. Therefore, a certain amount of coal fines is more likely to be retained inside the coal sample, yielding less fines production. Speaking of the backflow scenario (still in horizontal position), the originally stuck coal fines can be flushed away when the flow direction was reversed, contributing to more fines production (approximately 1×10^6 μm^3/mL) than the previous flat scenarios (0.35×10^6 μm^3/mL), as shown in Fig. 7.

Furthermore, a comparison between the two samples suggested that coal with higher initial permeability tended to yield more coal fines, because under the same pressure difference, greater permeability gave rise to higher flow velocity.

3.2 Coal fines particle size distribution

The particle size distribution of coal fines was measured for the effluents collected from each differential pressure using Coulter Counter. The cumulative percentage of volume for each pressure step was plotted as a function of particle size distribution in Fig. 9. Please note that the x-axis is on log scale.

Fig. 9. Particle size distribution of coal fines for various pressure differences.

For both samples, the sizes of the coal fine particles mainly range from 1 μm to 14 μm. The value of cumulative percentage of volume increases more rapidly for most curves at lower range, and gradually levels off with increasing particle sizes. This can be explained by (1) smaller coal fines require lower flow velocity to be mobilised, and can be flushed out of the sample more easily compared with larger fines; and (2) the cleat aperture limits the size of coal fines that can pass through these channels. In this study, the particle size at which the curvature experienced sudden change (i.e. the slope of the curve became less than 30) was defined as the critical particle size. No clear correlation between critical particle size and differential pressure was found, as illustrated in Fig. 10. A comparison between the total volume (Fig. 7) and critical particle size (Fig. 10) of the coal fines exhibits a similar trend, for example, they share the same peak points at certain pressure difference and similar fluctuation tendency for other data points, which verifies that the critical size is representative in terms of coal fines evaluation.

Fig. 10. Critical particle size of coal fines for (a) Sample 1 and (b) Sample 2.

3.3 Permeability evolution

The evolutions of coal permeability for both samples are illustrated in Fig. 11 and Fig. 12, respectively.

Fig. 11. Permeability evolution under different injection scenarios for Sample 1 (k_0=0.005 mD).

Fig. 12. Permeability evolution under different injection scenarios for Sample 2 (k_0=0.048 mD).

It can be seen that for both coal samples, during the water flooding process, the permeability dropped significantly (by 60.9% and 85%, respectively for Sample 1 and Sample 2 in the first 50 hours), followed by gradually decline with time, even if the differential pressure was increased. The variations in coal permeability can be explained by the counteraction of four phenomena: (1) the deposition and/or plugging of coal fines in cleats, damaging the permeability (i.e. entrapped coal fines); (2) the dilation of coal cleats by increased pore pressure (or decreased effective stress), resulting in permeability enhancement; (3) the discharge of coal fines widened the cleats, causing gradual permeability growth (i.e. coal fines production, data shown in Fig. 3); and (4) the unplugging, redistribution and/or recapture of coal fines due to local pressure build-up, contributing to permeability fluctuations. In phenomenon (1), the settlement of coal fines would lead to gradual permeability decline as a result of narrowed cleats (Pan and Connell, 2012), while the clogging would contribute to abrupt permeability deterioration due to closure of cleats.

Sample 1 witnesses more dramatic permeability fluctuations than Sample 2 resulted by coal fines behaviours. The explanation is that Sample 1 has narrower cleats with less connectivity compared with Sample 2 as evidenced by the SEM images (Fig. 2), therefore, more frequent entrapment, release and recapture of fines are expected (i.e. significant permeability fluctuations). On the other hand, more deposition and discharge of coal fines take place in wider and well-connect cleats (i.e. gradual permeability variations) (Civan, 2007). As gas has less carrying capacity of coal fines than water (Lyons et al., 2009), during the gas flooding process, the aforementioned phenomena (1), (3) and (4) only made a little difference in permeability change, consequently, coal permeability increased with rising differential pressure, which was dominated by phenomenon (2). It is suggested that during the stable gas production and the decline stages (i.e. single-phase gas flow takes place in CSG reservoirs), the Bottom-Hole Pressure (BHP) can be lowered to improve the gas productivity by enhancing the production pressure drawdown without introducing the permeability damage by coal fines.

Sample 2 produced greater coal fines, in terms of both volume and size. It also experienced more severe permeability damage during the same period. For instance, in the first 50 h, the permeability dropped by 60.9% and 85% respectively for Sample 1 and Sample 2, and in the first 100 h (shut-in periods for Sample 2 were accounted for), the permeability declined 79.1% and 88.2% for the two samples, respectively. However, in the CSG reservoirs, those with lower permeability are often facing with more severe coal fines problems. The possible reason is that the cleats in Sample 2 (Fig. 3a) are more tortuous than those in Sample 1 (Fig. 2a), and under the same pressure difference across the coal samples, more tortuous cleats generates localised pressure build-up. This enables higher flow velocity, causing larger viscous force around coal fines surface, which consequently creates more and larger coal fines.

Moreover, the impact of well shut-in on coal fines generation and migration was also simulated for Sample 2. A slight permeability loss was observed for every shut-in, which indicated that well shut-in has detrimental effects on coal permeability, as illustrated in the black dashed rectangle in Fig. 12. It is believed to be because the well shut-in provides sufficient time for coal fines to deposit, and the settled coal fines were more difficult to be remobilised than free fines, as it requires greater force to overcome the static inertial force (Khilar and Fogler, 1998; Zou et al., 2014). For example, Fig. 13 demonstrates that at 1.3 MPa, the two effluent samples from Sample 1 (collected consecutively without shut-in) coincide with each other quite well, which peak value at 1.2 μm. However, the peak of the particle size distribution from Sample 2 (with shut-in) shifts from 2.5 μm to 1.4 μm when analysing the second effluent, which indicates bigger coal fines are retained in the coal sample, deteriorating the permeability. In this concern, it can be inferred that larger coal fines settled down prior to smaller ones, and were more difficult to be removed when the flow was re-established. This indicates that by avoiding frequent well shut-in, coal fines caused permeability loss can be minimized, which is consistent with our previous finding (Bai et al., 2016; Bai et al., 2017).

Fig. 13. Particle size distribution of different effluent samples at 1.3 MPa. Note that “1” and “2” in the legend indicates the first and second effluent sample, respectively.

When gas was first introduced to both coal samples after the “1.5 MPa water” injection scenario, a sudden drop in the effective permeability ratio (i.e. from 0.119 to 0.056 for Sample 1, and from 0.121 to 0.048) is observed due to capillary resistance related to gas-drive-water two-phase flow, followed by effective permeability recovery after most water was expelled from the samples, as indicated by the red circles in Fig. 11 and Fig. 12. Such recovery is related to the increase of gas fraction in the samples, and the negligible movement of coal fines.

However, for the “1.5 MPa after gas” scenario of Sample 2, the permeability ratio dropped significantly (from 0.118 to 0.085) without noticeable bouncing back, as shown in the green circle in Fig. 12. According to the coal fines production data indicated by the red arrow in Fig. 7, the change of flow pattern from single-phase gas flow to water-drive-gas two-phase flow resulted in more coal fines generation, which in turn caused the permeability reduction. Since water-drive-gas two-phase flow normally occurs during production well shut-in, reducing the frequency of well shut-in can potentially minimize the coal fines induced permeability damage. Unlike the scenarios when coal sample is being vertically positioned, the permeability for the same sample when being the horizontally positioned stayed rather stable, which was corresponded to less coal fines production as shown in Fig. 7.

Regarding the scenarios after gas injection, by reducing the pressure difference, the permeability experienced step-like drop due to the reverse procedure of phenomenon (2), which was the closure of cleats. When the flow direction was reversed, a surge in permeability ratio is observed (from 0.034 to 0.043), as indicated by the yellow arrow in Fig. 12. This confirms that the permeability variations during the experiment are resulted by coal fines generation and migration.

Although theoretically the discharge of coal fines from the coal samples can bring up the permeability, according to the coal fines production data and the permeability evolution, more volume of coal fines production did not necessarily result in permeability improvement; on the contrary, more fines output was often associated with permeability declines. This was because with more coal fines production, the phenomenon of fines entrapment was also a matter of concern, which took the dominant role as explained earlier in this section.

4 CONCLUSIONS

A self-designed core flooding experimental rig was built to examine the coal fines induced permeability variations. Two cubic coal samples were tested under different pressures and flow regimes and the corresponding analysis was conducted on coal fines production (total volume and particle size distribution) and the corresponding permeability variations. The following main conclusions were drawn:

(1) Coal fines generation and migration are the dominant cause for the rapid reduction of coal permeability. The deposition and plugging of coal fines result in permeability loss; the removal of coal fines from the samples contributes to slight permeability enhancement; while the redistribution of coal fines give rise to permeability fluctuations.

(2) The coal fines volumetric production is proportional to the third power of flow velocity once the flow paths for coal fines are well established. The critical size coincides very well with the total volume of coal fines.

(3) Primary water flushing witnesses the most severe permeability damage due to coal fines generation and migration, the transition from single-phase gas flow to water-drive-gas flow lead to abrupt permeability loss, and pauses in the experiments introduce permeability drop because of coal fines settlement. It was also observed that the coal fines behaviours become negligible in single-phase gas flow.

(4) The coal sample with narrower and less connected cleating system causes more coal fines behaviours (i.e. entrapment, detachment and redistribution). This results in significant permeability fluctuations with general decreasing trend. Tortuosity of cleats can enhance the deterioration in permeability by coal fines behaviours.

These experimental results suggest that surfactant can be added to the reservoir through fracturing fluids to disperse coal fines, which makes it easier for water to flush small coal fines out, alleviating deposition and clogging induced permeability drop. During the early dewatering stage, the BHP should be properly controlled to reduce the drop speed of the dynamic fluid level. On the contrary, during the stable gas production phase, when only single-phase gas flow takes place, the BHP can be lowered rapidly to achieve higher gas productivity. Moreover, refraining from frequent well shut-in can ease coal fines damage towards the permeability as well.

ACKNOWLEDGEMENT

This work was partially supported by the top-up scholarship from Centre of Coal Seam Gas (CCSG) of the University of Queensland and State Key Laboratory of Coal Resources and Safe Mining at China University of Mining and Technology (Project No.: SKLCRSM16KFA03). These sources of support are gratefully acknowledged.

REFERENCES

Bagnold, R.A., 1936. The movement of desert sand. Proceedings of the Royal Society of London, Series A, Mathematical and Physical Sciences 157, 594-620.

Bai, T., Z. Chen, S.M. Aminossadati, N.N. Danesh, Z. Pan, J. Liu, L. Li, 2016. Impact of flow regimes on coal fines generation during Coal Seam Gas (CSG) production process, 50th US Rock Mechanics Geomechanics Symposium, Houston, Texas, USA.

Bai, T., Z. Chen, S.M. Aminossadati, L. Li, J. Liu, H. Lu, 2017. Dimensional analysis and prediction of coal fines generation under two-phase flow conditions. Fuel 194, 460-479.

Bai, T., Z. Chen, S.M. Aminossadati, Z. Pan, J. Liu, L. Li, 2015. Characterization of coal fines generation: A micro-scale investigation. Journal of Natural Gas Science and Engineering 27, Part 2, 862-875.

Bedrikovetsky, P., F. Siqueira, C. Furtado, A. Souza, 2011. Modified Particle Detachment Model for Colloidal Transport in Porous Media. Transp Porous Med 86, 353-383.

Black, D.J., 2011. Factors affecting the drainage of gas from coal and methods to improve drainage effectiveness, School of Civil, Mining and Environmental Engineering. University of Wollongong.

Chen, Z., J. Liu, D. Elsworth, L.D. Connell, Z. Pan, 2010. Impact of CO2 injection and differential deformation on CO2 injectivity under in-situ stress conditions. International Journal of Coal Geology 81, 97-108.

Civan, F., 2007. Particulate processes in porous media, in: Civan, F. (Ed.), Reservior formation damage. Elsevier, pp. 191-234.

Fu, X., Y. Qin, G.G.X. Wang, V. Rudolph, 2009. Evaluation of coal structure and permeability with the aid of geophysical logging technology. Fuel 88, 2278-2285.

Gash, B.W., 1991. Measurement of "Rock Properties" in Coal for Coalbed Methane Production, 66th Annual Technical Conference and Exhibition of the Society of Petroleum Engineers. Society of Petroleum Engineers, Dallas, TX, USA.

Guo, Z., F. Hussain, Y. Cinar, 2015. Permeability variation associated with fines production from anthracite coal during water injection. International Journal of Coal Geology 147–148, 46-57.

Guo, Z., F. Hussain, Y. Cinar, 2016. Physical and analytical modelling of permeability damage in bituminous coal caused by fines migration during water production. Journal of Natural Gas Science and Engineering.

Khilar, K.C., H.S. Fogler, 1998. Migration of fines in porous media. Springer.

Lyons, W.C., B. Guo, R.L. Graham, G.D. Hawley, 2009. Air and Gas Drilling Manual Applications for Oil and Gas Recovery Wells and Geothermal Fluids Recovery Wells, 3rd ed. Elsevier, Burlington, MA, USA.

Magill, D.P., M. Ramurthy, R. Jordan, P.D. Nguyen, 2010. Controlling Coal-Fines Production in Massively Cavitated Openhole Coalbed-Methane Wells. Society of Petroleum Engineers.

Marcinew, R.P., J.J. Hinkel, 1990. Coal Fines-Origin, Effects and Methods to Control Associated Damage, Annual Technical Meeting. Petroleum Society of Canada, Calgary, Alberta.

Moore, R.L., D.F. Loftin, I.D. Palmer, 2011. History Matching and Permeability Increases of Mature Coalbed Methane Wells in San Juan Basin, SPE Asia Pacific Oil and Gas Conference and Exhibition. Society of Petroleum Engineers, Jakarta, Indonesia.

Nimerick, K.H., J.J. Hinkel, K.W. England, J.L. Norton, M. Roy, 1990. Design and Evaluation of Stimulation and Workover Treatments in Coal Seam Reservoirs. Society of Petroleum Engineers, Calgary, Alberta, Canada.

Okotie, V.U., R.L. Moore, 2010. Well Production Challenges and Solutions in a Mature, Very Low-Pressure Coalbed Methane Reservoir, SPE Annual Technical Conference and Exhibition. Society of Petroleum Engineers, Florence.

Palmer, I.D., Z.A. Moschovidis, J.R. Cameron, 2005. Coal failure and consequences for coalbed methane wells, SPE Annual Technical Conference and Exhibition. Society of Petroleum Engineers, Dallas, Texas.

Pan, Z., L.D. Connell, 2012. Modelling permeability for coal reservoirs: A review of analytical models and testing data. International Journal of Coal Geology 92, 1-44.

Wang, C., P. Zhai, Z. Chen, J. Liu, L. Wang, J. Xie, 2017. Experimental study of coal matrix-cleat interaction under constant volume boundary condition. International Journal of Coal Geology.

Wei, C., M. Zou, Y. Sun, Z. Cai, Y. Qi, 2015. Experimental and applied analyses of particle migration in fractures of coalbed methane reservoirs. Journal of Natural Gas Science and Engineering 23, 399-406.

Wei, Y., D. Cao, Y. Yuan, X. Zhu, Z. Yao, J. Zhou, 2013. Characteristics and controlling factors of pulverized coal during coalbed methane drainage in Hancheng area. Journal of China Coal Society 38, 1424-1429.

Yao, Z., D. Cao, Y. Wei, X. Li, X. Wang, X. Zhang, 2016. Experimental analysis on the effect of tectonically deformed coal types on fines generation characteristics. Journal of Petroleum Science and Engineering 146, 350-359.

Zhao, X., S. Liu, S. Sang, Z. Pan, W. Zhao, Y. Yang, Q. Hu, Y. Yang, 2016. Characteristics and generation mechanisms of coal fines in coalbed methane wells in the southern Qinshui Basin, China. Journal of Natural Gas Science and Engineering 34, 849-863.

Zhao, Y., Y. Sun, S. Liu, K. Wang, Y. Jiang, 2017. Pore structure characterization of coal by NMR cryoporometry. Fuel 190, 359-369.

Zou, Y.S., S.C. Zhang, J. Zhang, 2014. Experimental Method to Simulate Coal Fines Migration and Coal Fines Aggregation Prevention in the Hydraulic Fracture. Transp Porous Med 101, 17-34.

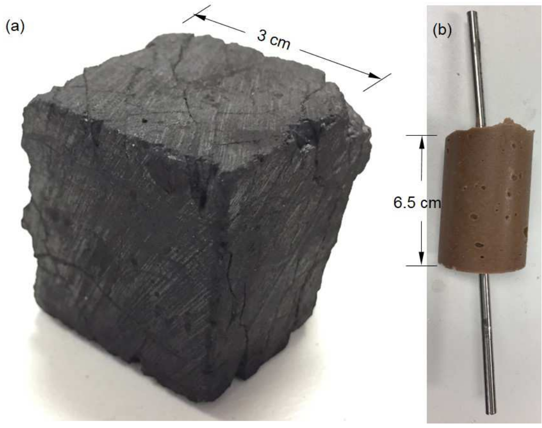
(a)
3 cm
(b)
6.5 cm

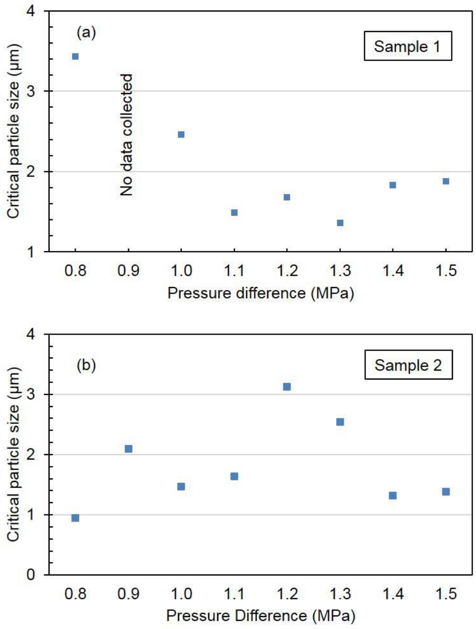
(a)
Sample 1
Critical particle size (μm)
No data collected
Pressure difference (MPa)
4
3
2
1
0.8
0.9
1.0
1.1
1.2
1.3
1.4
1.5
(b)
Sample 2
Critical particle size (μm)
Pressure Difference (MPa)
4
3
2
1
0

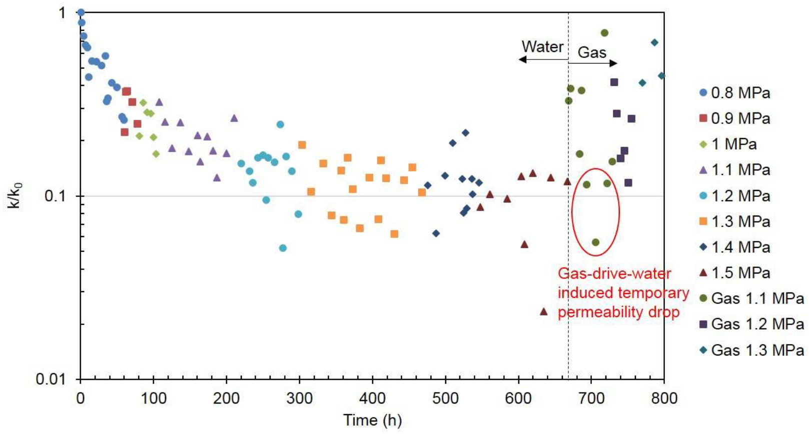

1
0.1
0.01
k/k0
0
100
200
300
400
500
600
700
800
Time (h)
Water
Gas
Gas-drive-water
induced temporary
permeability drop
0.8 MPa
0.9 MPa
1 MPa
1.1 MPa
1.2 MPa
1.3 MPa
1.4 MPa
1.5 MPa
Gas 1.1 MPa
Gas 1.2 MPa
Gas 1.3 MPa

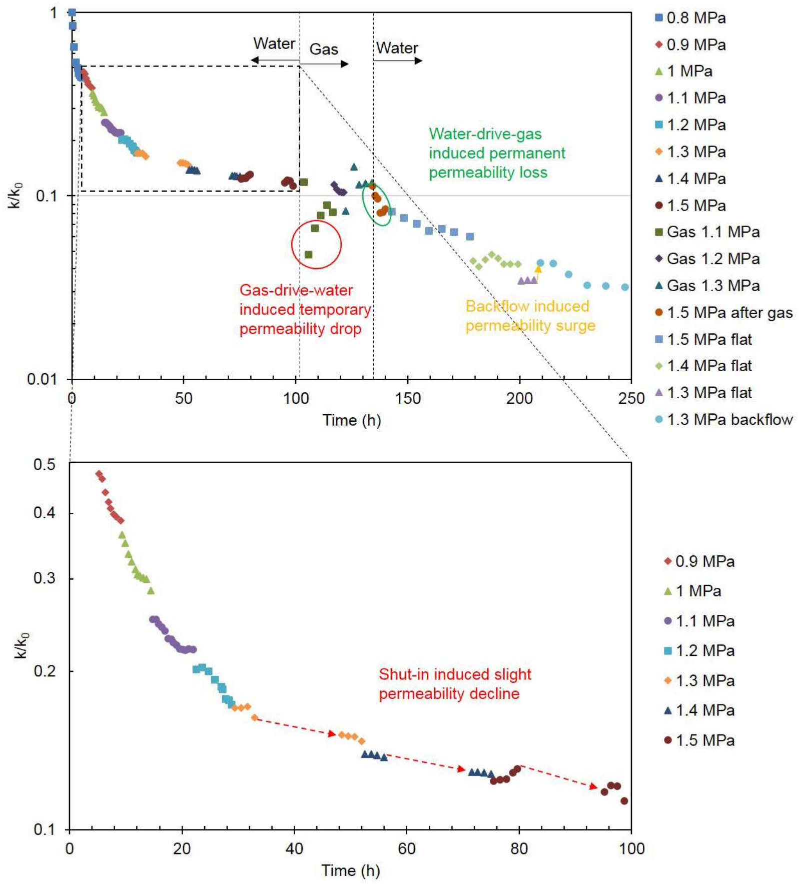

1
0.1
0.01
k/k0
Water
Gas
Water
Water-drive-gas induced permanent permeability loss
Gas-drive-water induced temporary permeability drop
Backflow induced permeability surge
0
50
100
150
200
250
Time (h)
0.8 MPa
0.9 MPa
1 MPa
1.1 MPa
1.2 MPa
1.3 MPa
1.4 MPa
1.5 MPa
Gas 1.1 MPa
Gas 1.2 MPa
Gas 1.3 MPa
1.5 MPa after gas
1.5 MPa flat
1.4 MPa flat
1.3 MPa flat
1.3 MPa backflow
0.5
0.4
0.3
0.2
0.1
k/k0
Shut-in induced slight permeability decline
0
20
40
60
80
100
Time (h)
0.9 MPa
1 MPa
1.1 MPa
1.2 MPa
1.3 MPa
1.4 MPa
1.5 MPa

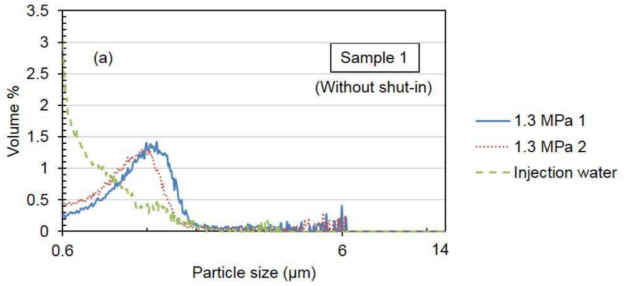

3.5
3
2.5
2
1.5
1
0.5
0
Volume %
(a)
Sample 1
(Without shut-in)
0.6
6
14
Particle size (μm)
1.3 MPa 1
1.3 MPa 2
Injection water

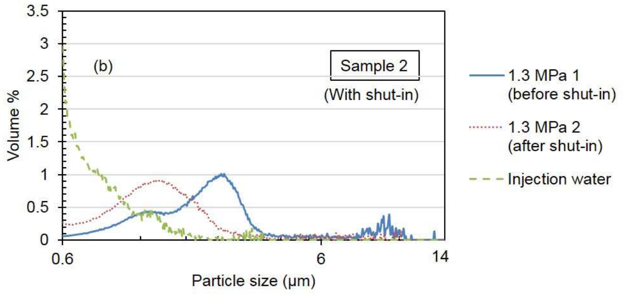

3.5
3
2.5
2
1.5
1
0.5
0
Volume %
(b)
Sample 2
(With shut-in)
0.6
6
14
Particle size (μm)
1.3 MPa 1
(before shut-in)
1.3 MPa 2
(after shut-in)
Injection water

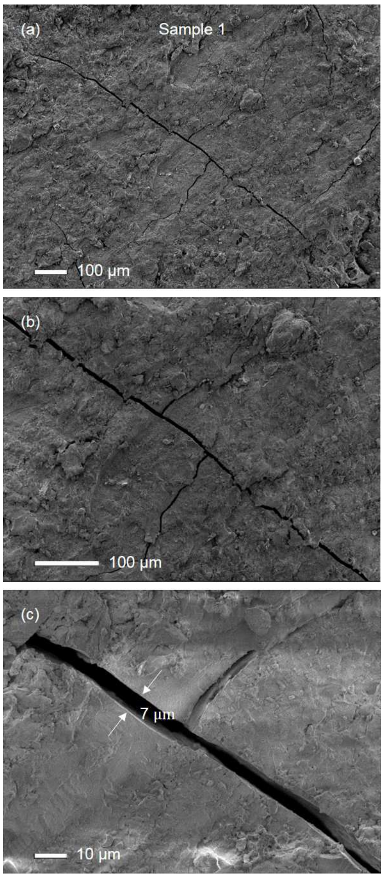
(a)
Sample 1
100 µm
(b)
100 µm
(c)
7 µm
10 µm

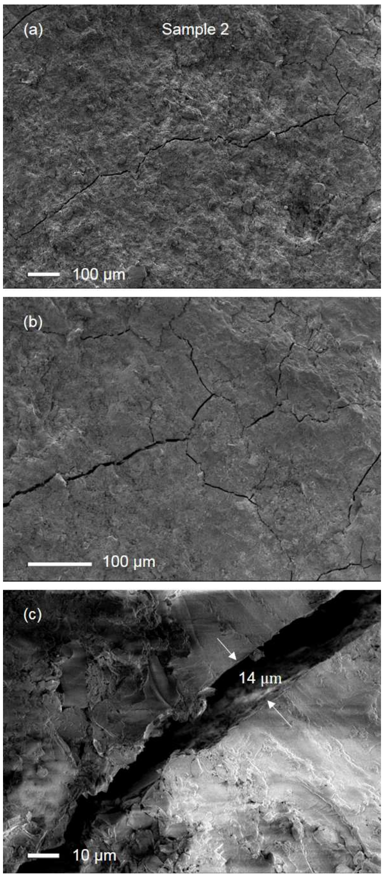
(a)
Sample 2
100 μm
(b)
100 μm
(c)
14 μm
10 μm

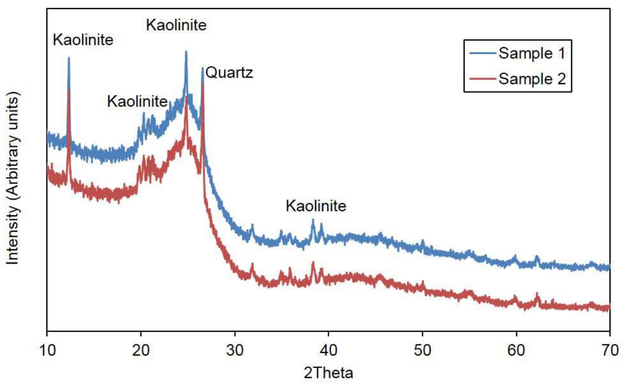
Kaolinite
Kaolinite
Kaolinite
Quartz
Kaolinite
Sample 1
Sample 2
Intensity (Arbitrary units)
10
20
30
40
50
60
70
2Theta

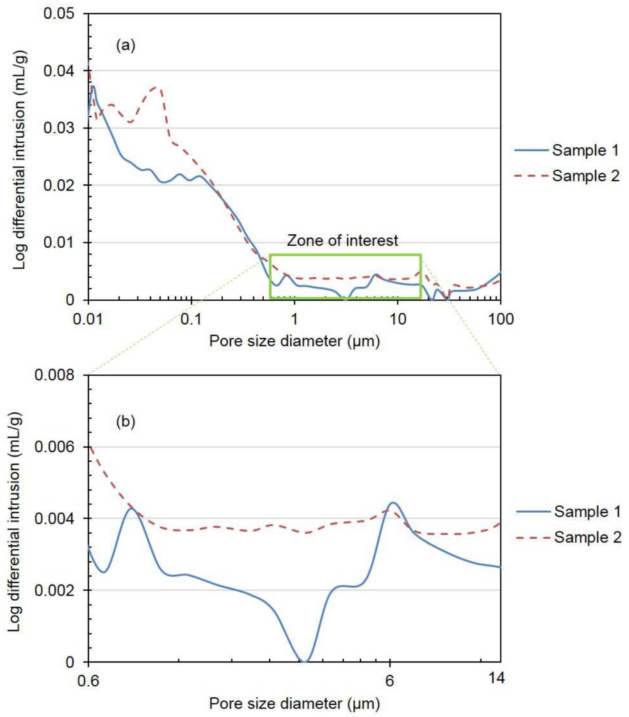

0.05
0.04
0.03
0.02
0.01
0
(a)
Log differential intrusion (mL/g)
Zone of interest
0.01
0.1
1
10
100
Pore size diameter (μm)
Sample 1
Sample 2
0.008
0.006
0.004
0.002
(b)
0.6
6
14

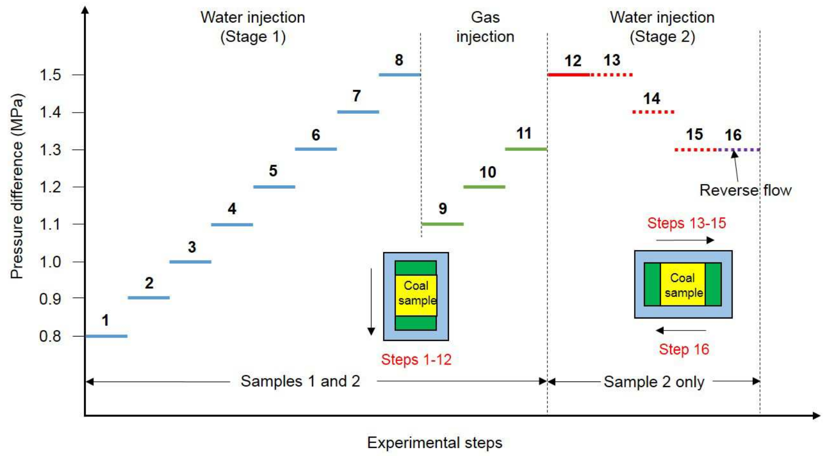

Water injection
(Stage 1)
Gas
injection
Water injection
(Stage 2)
Pressure difference (MPa)
1.5
1.4
1.3
1.2
1.1
1.0
0.9
0.8
1
2
3
4
5
6
7
8
9
10
11
12
13
14
15
16
Reverse flow
Steps 13-15
Coal
sample
Step 16
Steps 1-12
Samples 1 and 2
Sample 2 only
Experimental steps

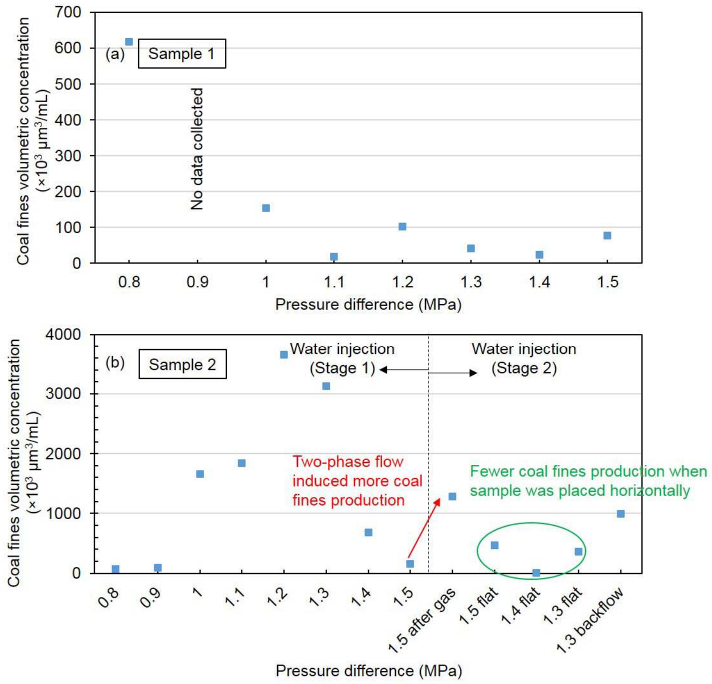

700
600
500
400
300
200
100
0
(a)
Sample 1
No data collected
Coal fines volumetric concentration (×10³ μm³/mL)
0.8
0.9
1
1.1
1.2
1.3
1.4
1.5
Pressure difference (MPa)
4000
3000
2000
1000
0
(b)
Sample 2
Water injection (Stage 1)
Water injection (Stage 2)
Two-phase flow induced more coal fines production
Fewer coal fines production when sample was placed horizontally
Coal fines volumetric concentration (×10³ μm³/mL)
0.8
0.9
1
1.1
1.2
1.3
1.4
1.5
1.5 after gas
1.5 flat
1.4 flat
1.3 flat
1.3 backflow
Pressure difference (MPa)

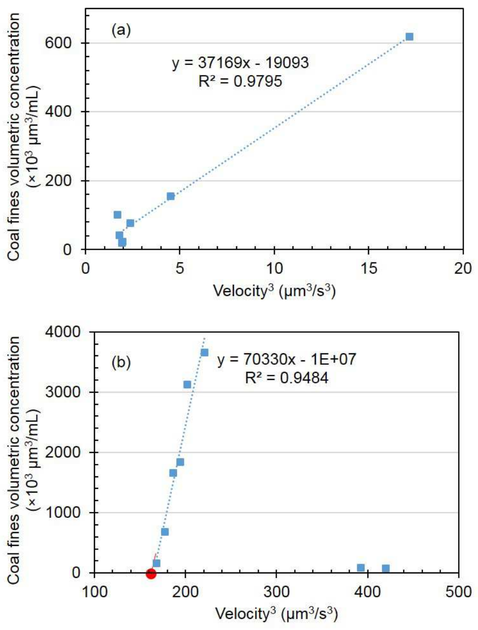

(a)
y = 37169x - 19093
R² = 0.9795
Coal fines volumetric concentration (×10³ μm³/mL)
Velocity³ (μm³/s³)
0
200
400
600
0
5
10
15
20
(b)
y = 70330x - 1E+07
R² = 0.9484
Coal fines volumetric concentration (×10³ μm³/mL)
Velocity³ (μm³/s³)
0
1000
2000
3000
4000
100
200
300
400
500

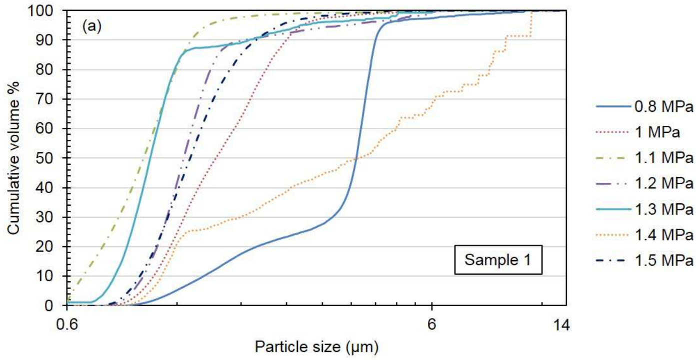
(a)
Cumulative volume %
Particle size (µm)
Sample 1
0.8 MPa
1 MPa
1.1 MPa
1.2 MPa
1.3 MPa
1.4 MPa
1.5 MPa

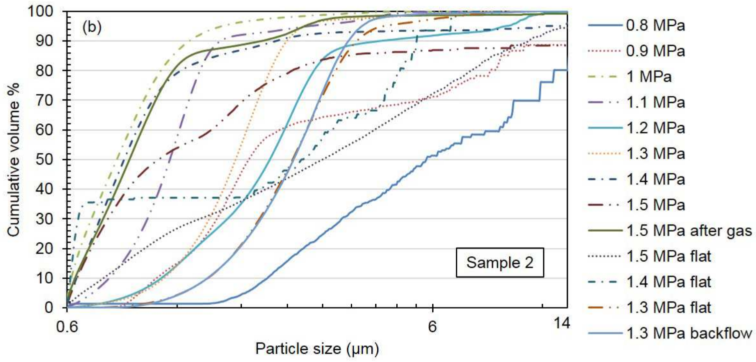
(b)
Cumulative volume %
Particle size (µm)
Sample 2
0.8 MPa
0.9 MPa
1 MPa
1.1 MPa
1.2 MPa
1.3 MPa
1.4 MPa
1.5 MPa
1.5 MPa after gas
1.5 MPa flat
1.4 MPa flat
1.3 MPa flat
1.3 MPa backflow

Highlights:

- Coal permeability variations induced by coal fines were quantified;
- Impact of cleat characteristics on fines-permeability relationship was investigated;
- Characterization of coal fines output in different production stages was conducted;
- Guidelines were suggested to minimize production loss induced by coal fines.